EPR investigations of intermediate Jahn-Teller coupling effects for Cu^{2+} in MgO and CaO

R. W. Reynolds and L. A. Boatner
Advanced Technology Center, Incorporated, Dallas, Texas 75222*

M. M. Abraham and Y. Chen
Solid State Division, Oak Ridge National Laboratory,† Oak Ridge, Tennessee 37830

(Received 20 May 1974)

The electron-paramagnetic-resonance (EPR) spectra of divalent copper in CaO and MgO single crystals have been observed at 1.2 and 77 K. Although the basic characteristics of the low-temperature (1.2 K) Cu^{2+} spectra in these hosts were somewhat similar to those resulting from a dynamic Jahn-Teller effect, significant deviations in the line shapes and angular variations were found. For $CaO:Cu^{2+}$, the angular variations in the $\{110\}$ and $\{001\}$ planes due to both the Zeeman and hyperfine interactions were fully consistent with the properties of a ^2E vibronic ground state with appreciable random-strain coupling to an excited A_1 vibronic singlet (i.e., an intermediate Jahn-Teller effect). A numerical diagonalization of the matrix of random strain and tunneling within the A_1 and ^2E manifold was performed for various ratios of average random-strain splitting $\bar{\delta}$ to tunneling splitting 3Γ, and the corresponding EPR spectra were computed. The calculated line shapes and angular variations were then compared with the experimental results. For Cu^{2+} in CaO, a value of $\bar{\delta}/3\Gamma = 0.67$ was obtained; and this value together with the effective spin-Hamiltonian parameters for the isolated ^2E state describes both the complete angular variation and the details of the asymmetric line shapes found for $\vec{H} \| [111]$. From this value of $\bar{\delta}/3\Gamma$ and a recently published value for 3Γ, we find that $\bar{\delta} = 2.7\ cm^{-1}$ for $CaO:Cu^{2+}$. In contrast to the $CaO:Cu^{2+}$ results, the $MgO:Cu^{2+}$ EPR spectrum exhibited the effects of random-strain coupling to an excited A_2 vibronic singlet. Although a value of $\bar{\delta}/3\Gamma$ could be determined which described the angular variation of the Zeeman interaction, the angular dependence of the hyperfine structure and the line shapes observed for $\vec{H} \| [111]$ were not consistent with this $\bar{\delta}/3\Gamma$ value. For Cu^{2+} in MgO, the experimental results strongly suggest that random-strain coupling to both the A_1 and A_2 vibronic singlets is responsible for the observed discrepancies.

I. INTRODUCTION

Previous investigations of ^2E orbital states of ions in cubic-symmetry hosts have shown that the associated low-temperature electron-paramagnetic-resonance (EPR) spectra may be characteristic of a Jahn-Teller (JT) effect which in general can be classified as either "static" or "dynamic."[1] Excluding hyperfine structure, the EPR spectra of those systems associated with a static JT effect at low temperature are composed of three magnetically inequivalent axially symmetric resonance lines whose principal symmetry axes lie along the fourfold symmetry axes of the cubic host. As the temperature increases, these axially symmetric resonance lines are motionally averaged to produce a single isotropic resonance with $g = \frac{1}{3}(g_{\parallel} + 2g_{\perp})$ where $g_{\parallel}$ and $g_{\perp}$ describe the low-temperature spectrum. Numerous examples of the static JT effect have been reported previously. These include Cu^{2+} in NaCl, LiCl, and NaF (Refs. 2 and 3); Ni^{1+} in NaCl, LiF, and CaO (Refs. 3–5); and Y^{2+} and La^{2+} in CaF_2 (Refs. 6 and 7).

For ^2E orbital states in cubic symmetry, the EPR spectrum associated with a dynamic JT effect at low temperature is characterized (again excluding hyperfine structure) by the presence of a single strain-broadened resonance line.[1,8] At orientations of the applied magnetic field other than $\vec{H} \| \langle 111 \rangle$, the resonance line shape has two absorption peaks with one of these peaks occurring on either side (or magnetic-field extreme) of the line. The magnetic-field positions of the peaks of this line exhibit a cubic-symmetry variation depending on the orientation of the applied magnetic field relative to the cubic axes of the host. The greatest separation of the magnetic-field positions of the peaks occurs when the applied magnetic field is parallel to one of the fourfold cubic axes, and the peaks coincide when the field is parallel to one of the $\langle 111 \rangle$ axes. As the temperature increases, the anisotropic spectrum is replaced by a single isotropic line whose magnetic-field position coincides with that of the coincident peaks of the anisotropic spectrum at $\vec{H} \| \langle 111 \rangle$. This isotropic line is due to population of an excited vibronic singlet level or to averaging by vibronic relaxation of a portion of the anisotropic spectrum.[9] Examples of systems displaying a low-temperature dynamic JT effect are Sc^{2+} in CaF_2, SrF_2, BaF_2, and $SrCl_2$ (Refs. 10–12); La^{2+} in $SrCl_2$ (Ref. 13); and Y^{2+} in $SrCl_2$ (Ref. 12).

Theoretical treatments by Ham[1] and Chase[14] have indicated that the type of low-temperature JT ef-

fect observed for ^2E orbital states in cubic symmetry is dependent on the relative strengths of the JT coupling and the random strain present in the crystal. In fact, they have shown that the static and dynamic JT effects, which were identified in the early EPR investigations, actually represent only the two limiting cases of a continuous variation of possible JT effects. Whether dynamic, static, or intermediate JT effects are observed depends on the ratio $\bar{\delta}/3\Gamma$, where $\bar{\delta}$ is the average splitting due to random strain of the ground state and 3Γ is the "tunneling" splitting between the ground state and next excited vibronic singlet level of the system. This "tunneling" splitting depends inversely on the JT coupling strength. For small values of $\bar{\delta}/3\Gamma$, purely dynamic JT effects are observed while for large values of this ratio, static JT effects occur.

Until recently, no experimental observations for ^2E orbital ground states in cubic symmetry had been reported which were characteristic of intermediate JT coupling. (An intermediate JT effect had, however, been identified by Chase[14] for an excited Γ_8 level of Eu^{2+} in CaF_2.) Recently, we reported that intermediate JT effects were present in the EPR spectra due to the ground ^2E level of Ag^{2+} in MgO and CaO.[15-17] In particular, it was determined that at low temperature the JT effect is static for SrO : Ag^{2+}, predominately static but intermediate to the dynamic effect for CaO : Ag^{2+}, and predominately dynamic but slightly intermediate to the static effect for MgO : Ag^{2+}. In each host crystal the observed features of the spectra were in agreement with the predictions of the theory of Ham[1] and Chase[14] which describe the transition from dynamic to static JT effects. Moreover, for MgO : Ag^{2+} and CaO : Ag^{2+} values for $\bar{\delta}$ and 3Γ were determined. Since Cu^{2+} and Ag^{2+} should have analogous electronic properties in the alkaline-earth oxide hosts, we have subsequently investigated Cu^{2+} in MgO and CaO[18] and have discovered intermediate JT coupling effects in the EPR spectra of these systems. The purpose of this paper is to present the results of this investigation.

In order to understand how the characteristics of the CaO : Cu^{2+} and MgO : Cu^{2+} EPR spectra depart from those associated with dynamic or static JT effects, it will be necessary to describe the origins and characteristics of the static and dynamic JT effects. This explanation is the subject of the following section (Sec. II). Additionally, the theory of Ham and Chase which describes the transition from dynamic to static JT effects will be presented in Sec. II, and the implications of this theory for the EPR spectra of systems with intermediate JT coupling will be developed. A brief summary of previous EPR investigations of CaO : Cu^{2+} and MgO : Cu^{2+} will be given in Sec. III. In Sec. IV, it will be shown that calculations based on the theory of Ham and Chase explain in detail the unusual properties of the CaO : Cu^{2+} EPR spectrum. Values of $\bar{\delta}$ and 3Γ determined for CaO : Cu^{2+} will be compared with similar results for Ag^{2+} in the alkaline-earth oxides. A justification for the inability of a similar calculation to fully explain the MgO : Cu^{2+} EPR spectrum is also given.

II. THEORY

The effect of linear JT coupling on a ^2E electronic state in cubic symmetry can be expressed by means of the following effective Hamiltonian[1]:

$$\mathcal{H}_v = E_0\mathcal{T} + V(Q_\theta \mathfrak{U}_\theta + Q_\epsilon \mathfrak{U}_\epsilon) + \tfrac{1}{2}K(Q_\theta^2 + Q_\epsilon^2)\mathcal{T} \ . \qquad (1)$$

Here E_0 is the electronic energy of the ^2E state in the absence of any lattice distortion, V is the linear JT coupling coefficient, Q_θ and Q_ϵ are lattice distortion coordinates transforming as the θ and ϵ components of the E irreducible representation of O_h, K is an effective lattice elastic constant, and $\mathcal{T}$, $\mathfrak{U}_\theta$, and $\mathfrak{U}_\epsilon$ are orbital electronic operators, having the matrix form

$$\mathcal{T} = \begin{bmatrix} +1 & 0 \\ 0 & +1 \end{bmatrix} ; \quad \mathfrak{U}_\theta = \begin{bmatrix} -1 & 0 \\ 0 & +1 \end{bmatrix}$$
$$\mathfrak{U}_\epsilon = \begin{bmatrix} 0 & +1 \\ +1 & 0 \end{bmatrix} , \qquad (2)$$

with respect to the Ψ_θ and Ψ_ϵ electronic basis states. Since the ionic kinetic energy is considered small enough to be omitted from Eq. (1), the Born–Oppenheimer approximation is assumed valid. Here Q_θ and Q_ϵ represent essentially static distortions of the cluster composed of the JT ion and its nearest neighbors, and these distortions are assumed to be more effective in producing JT splittings than the distortions associated with the continuum of lattice phonons.

Solutions to Eq. (1) were found by Van Vleck[19] who showed that the electronic degeneracy of the ^2E state was removed with the minimum energy of the system occurring for the infinite number of distortions for which

$$(Q_\theta^2 + Q_\epsilon^2)^{1/2} = |V|/K \ . \qquad (3)$$

The energy decrease from E_0 is known as the JT stabilization energy $E_{JT} = V^2/2K$.

Other investigators (Liehr and Ballhausen,[20] Opik and Pryce[21]) have added to Eq. (1) the following nonlinear JT coupling terms whose transformation properties are still consistent with a cubic complex:

$$V_q[(Q_\epsilon^2 - Q_\theta^2)\mathfrak{U}_\theta + 2Q_\epsilon Q_\theta \mathfrak{U}_\epsilon] + V_c Q_\theta (Q_\theta^2 - 3Q_\epsilon^2)\mathcal{T} \ , \qquad (4)$$

where V_q and V_c are, respectively, the quadratic vibronic coupling and anharmonic lattice force con-

stant parameters. If these so-called "warping" terms are sufficiently large, they have the effect of stabilizing only those distorted configurations corresponding to compressions or elongations along the cubic axes to produce the static JT effect.

The first theoretical investigations of low-temperature dynamic JT effects in EPR spectra were those of Bersuker[22,23] and O'Brien.[24] Starting with the above static formulation, they determined the effect on the EPR spectra of varying the barrier height between the distorted configurations produced by the "warping terms." Lowering the barrier height allowed tunneling of the system between distorted configurations with a resulting change in the ground-state expectation values of the Zeeman and hyperfine interactions. These calculations, however, are only applicable to those systems meeting the assumption implicit in Eq. (1); i.e., that the JT coupling is sufficiently large relative to the lattice phonon energies that the ground-state vibronic wave functions contain only the lower of the two electronic states resulting from the JT splitting. Additionally these calculations have not included the effect of random strain on the vibronic ground state. Ham[1] has estimated that the random strain should produce an effect at least comparable to that of the Zeeman interaction.

For systems in which the JT coupling is weak to moderate, Ham[1,8,25] has extended the work by Moffitt *et al.*,[26] and Longuet-Higgins, *et al.*,[27] to predict the nature of the JT effects present in the EPR spectra of such systems. Since this formulation can also incorporate strong JT coupling effects, we have found Ham's treatment most convenient for describing the wide range of JT effects present in the EPR spectra of d^9-configuration ions in the alkaline-earth oxides. For weak JT coupling, the Born–Oppenheimer approximation is no longer considered valid, and the nuclear kinetic-energy operators are included in Eq. (1) where Q_θ and Q_ϵ are considered as coordinates for the appropriate E modes of vibration of the cluster. Here again the contribution to the coupling from the continuum of lattice-vibrational modes is ignored. If the angular frequency corresponding to the E mode is designated as ω, and the effective mass by μ, then the force constant K is given by $\mu\omega^2$ and E_{JT} by $V^2/2\mu\omega^2$. With the addition of the nuclear-kinetic-energy terms, the vibronic eigenstates and eigenvalues of Eq. (1) can no longer be obtained analytically. However, since the Hamiltonian must still retain the full cubic symmetry of the system under appropriate transformations, its eigenstates must belong to the same irreducible representations of O_h as those determined in the absence of JT coupling. For all values of the linear coupling parameter V, the ground state is then found to be a vibronic ^2E level while the first excited state is an accidentally degenerate doublet transforming as A_1 and A_2. If these excited states are separated from the ground state by an energy difference that is large relative to any external perturbations, then as shown by Ham[8,25] the effect of these perturbations on the ^2E ground vibronic doublet can be represented by the following operator:

$$\mathcal{H}_\gamma = G_1\mathcal{T}_\gamma + pG_2A_{\gamma 2} + q(G_\theta \mathfrak{U}_{\gamma\theta} + G_\epsilon \mathfrak{U}_{\gamma\epsilon}) , \tag{5}$$

where G_1, G_2, G_θ, and G_ϵ are functions of the relevant external perturbations and spin operators (but are independent of Q_θ and Q_ϵ) and transform, respectively, as the A_1, A_2, E_θ, and E_ϵ irreducible representations of the O_h point group. The Hamiltonian operators $\mathcal{T}_\gamma$, $\mathfrak{U}_{\gamma\theta}$, and $\mathfrak{U}_{\gamma\epsilon}$ have the same matrix elements as in Eq. (2) relative to the ground vibronic-basis wave functions $\Psi_{\gamma\theta}$ and $\Psi_{\gamma\epsilon}$. The operator $A_{\gamma 2}$ is given by

$$A_{\gamma 2} = \begin{bmatrix} 0 & -i \\ +i & 0 \end{bmatrix} ,$$

relative to the same basis. The dimensionless "reduction factors" p and q represent the change in the expectation value of each term in Eq. (5) due to the presence of vibronic coupling. Quantitatively, they are given by

$$q = -\langle \Psi_{\gamma\theta} | \mathfrak{U}_\theta | \Psi_{\gamma\theta} \rangle = \langle \Psi_{\gamma\epsilon} | \mathfrak{U}_\theta | \Psi_{\gamma\epsilon} \rangle = \langle \Psi_{\gamma\epsilon} | \mathfrak{U}_\epsilon | \Psi_{\gamma\theta} \rangle , \tag{6}$$

$$p = i\langle \Psi_{\gamma\theta} | A_2 | \Psi_{\gamma\epsilon} \rangle .$$

For zero JT coupling, $p = q = 1$. For strong JT coupling, $p \simeq 0$ and $q \simeq \frac{1}{2}$. If only linear JT coupling is present, $q = \frac{1}{2}(1+p)$. Values for p and q for various intermediate values of JT coupling strengths have been calculated by different authors, and are summarized in the article by Ham.[1]

For electron-paramagnetic-resonance investigations, the pertinent operators in Eq. (5) include, first, the terms

$$G_\theta = V_2 e_\theta , \quad G_\epsilon = V_2 e_\epsilon , \tag{7}$$

which account for the effects of random strain in the crystal (here V_2 is the strain-coupling parameter and e_θ and e_ϵ are the strain components transforming, respectively, as the θ and ϵ components of the E irreducible representation), and, second, the Zeeman and hyperfine interactions which are represented in the following relations:

$$G_1 = g_1\mu_B \vec{H}\cdot\vec{S} + A_1 \vec{I}\cdot\vec{S} ,$$

$$G_\theta = \tfrac{1}{2} g_2\mu_B (3H_\gamma S_\gamma - \vec{H}\cdot\vec{S}) + \tfrac{1}{2}A_2(3I_\gamma S_\gamma - \vec{I}\cdot\vec{S}) , \tag{8}$$

$$G_\epsilon = \tfrac{1}{2}\sqrt{3}\, g_2\mu_B (H_x S_x - H_y S_y)$$

$$+\tfrac{1}{2}\sqrt{3}\,A_2(I_xS_x - I_yS_y)\ .$$

Substitution of the operators of Eq. (7) and (8) into Eq. (5) results in an effective Hamiltonian for the system. Second-order solutions to this Hamiltonian have been given previously by Herrington, Estle, and Boatner[12] for the case where the random strains are sufficiently large to determine the eigenstates, and have been shown to describe accurately the EPR spectra of many d^1 configuration ions (e.g., Sc^{2+} in the alkaline-earth fluorides[11] La^{2+}, Y^{2+}, and Sc^{2+} in $SrCl_2$).[12,13]

If the strain interaction determines the composition of the vibronic states, then the solutions to Eq. (5) for the strain and Zeeman interactions only are given by the expression

$$E_{\pm,M_S} = \pm q V_2(e_\theta^2 + e_\epsilon^2)^{1/2} + g_1\mu_B H M_S \times [1 \pm (qg_2/g_1)f_1 + (qg_2/g_1)^2 f_2]^{1/2}\ , \tag{9}$$

where

$$f_1 = (3n^2 - 1)\cos\phi + \sqrt{3}\,(l^2 - m^2)\sin\phi\ ,$$
$$f_2 = \tfrac{1}{2} + \tfrac{1}{4}(3n^2 - 1)\cos 2\phi - \tfrac{1}{4}\sqrt{3}\,(l^2 - m^2)\sin 2\phi\ , \tag{10}$$
$$\tan\phi = e_\epsilon/e_\theta\ ,$$

and l, m, and n are the direction cosines of the magnetic field relative to the cubic axes. The subscript (±) differentiates the solutions for the strain-determined eigenstates which are given by the expression:

$$\Psi_+ = \sin(\tfrac{1}{2}\phi)\Psi_{g\theta} + \cos(\tfrac{1}{2}\phi)\Psi_{g\epsilon}\ ,$$
$$\Psi_- = \cos(\tfrac{1}{2}\phi)\Psi_{g\theta} - \sin(\tfrac{1}{2}\phi)\Psi_{g\epsilon}\ . \tag{11}$$

The allowed ($\Delta M_S = \pm 1$) EPR transitions occur at the magnetic-field strengths given by the expression

$$H_\pm = (h\nu/g_1\mu_B)[1 \pm (qg_2/g_1)f_1 + (qg_2/g_1)^2 f_2]^{-1/2}\ . \tag{12}$$

Including the hyperfine and quadrupole interactions, the corresponding second-order relationship (expressed in terms of frequency) is as follows[13,28]:

$$h\nu_\pm = \left(g_1 \pm \tfrac{1}{2}qg_2f_1 + \frac{(qg_2)^2}{g_1}f_3\right)\mu_B H + \left(A_1 \pm \tfrac{1}{2}qA_2f_1 + \frac{(qA_2)^2}{A_1}f_3 + 2\frac{qg_2}{g_1}qA_2f_3 + \frac{4(qQ)^2}{A_1}[(f_3 - f_4) + 2(f_4 - 2f_3)I(I+1)]\right)M_I + \left(\frac{(A_1 \mp \tfrac{1}{4}qA_2f_1)^2}{2g_1\mu_B H} + \frac{(qA_2)^2}{g_1\mu_B H}f_4\right)[I(I+1) - M_I^2] + \frac{(qA_2)^2}{g_1\mu_B H}f_3M_I^2 + \frac{8(qQ)^2}{A_1}(2f_3 - f_4)M_I^3\ , \tag{13}$$

where

$$f_3 = \tfrac{1}{8}\{2 - [(3n^2 - 1)\cos\phi + \sqrt{3}\,(l^2 - m^2)\sin\phi]^2 - [-(3n^2 - 1)\cos 2\phi + \sqrt{3}\,(l^2 - m^2)\sin 2\phi]\}\ ,$$
$$f_4 = \tfrac{1}{32}\{4 + [(3n^2 - 1)\cos\phi + \sqrt{3}\,(l^2 - m^2)\sin\phi]^2 + 4[-(3n^2 - 1)\cos 2\phi + \sqrt{3}\,(l^2 - m^2)\sin 2\phi]\}\ . \tag{14}$$

The effect of random strain is to distribute the EPR transitions between the extremes determined by Eq. (12). This distribution of EPR transitions produces a spectrum which has the appearance of an EPR powder spectrum. The distribution of strain between the θ and ϵ components is generally assumed to be uniform, and accordingly all values of ϕ (where $\tan\phi = e_\epsilon/e_\theta$) between 0 and 2π are usually assumed to be equally likely. The linewidth of the complete absorption spectrum displays cubic-symmetry anisotropy, and, since most EPR spectrometers record the first derivative of the absorption, the observed spectrum for a general orientation of the applied field consists of two anisotropic and asymmetric resonance lines. The JT effect in these spectra is evidenced only by departures of q from unity.

As the linear JT coupling term is increased relative to $\hbar\omega$, the energy separation between the ^2E ground state and the degenerate A_1 and A_2 levels decreases and, for sufficiently large JT coupling, the the ^2E and A_1, A_2 levels approach degeneracy. The addition of "warping" terms [Eq. (4)] removes the A_1, A_2 degeneracy. When the separation of the ^2E and either the A_1 or A_2 levels becomes comparable to the effects of external perturbations (e.g., random strain and anisotropic Zeeman interactions), appreciable admixture of these states may occur. This admixture marks the onset of intermediate JT effects and ultimately results in a static JT effect.

If only one of the excited singlets is close to the ^2E ground state, the generalized Hamiltonian $\mathcal{H}$ takes the following matrix form[1] with respect to the Ψ_{A1}, $\Psi_{g\theta}$, and $\Psi_{g\epsilon}$ basis:

$$\begin{pmatrix} 3\Gamma + G_1 & rG_\theta & rG_\epsilon \\ rG_\theta & G_1 - qG_\theta & qG_\epsilon \\ rG_\epsilon & qG_\epsilon & G_1 + qG_\theta \end{pmatrix} \tag{15}$$

for the A_1 vibronic singlet lower, or (with respect to Ψ_{A2}, $\Psi_{g\theta}$, and $\Psi_{g\epsilon}$)

$$\begin{pmatrix} 3\Gamma + G_1 & rG_\epsilon & -rG_\theta \\ rG_\epsilon & G_1 - qG_\theta & qG_\epsilon \\ -rG_\theta & qG_\epsilon & G_1 + qG_\theta \end{pmatrix} \tag{16}$$

for the A_2 vibronic singlet lower. Here

$$r = \langle \Psi_{A1} | \mathcal{U}_\theta | \Psi_{g\theta} \rangle = \langle \Psi_{A1} | \mathcal{U}_\epsilon | \Psi_{g\epsilon} \rangle , \tag{17}$$

or

$$r = \langle \Psi_{A2} | \mathcal{U}_\epsilon | \Psi_{g\theta} \rangle = -\langle \Psi_{A2} | \mathcal{U}_\theta | \Psi_{g\epsilon} \rangle ,$$

and 3Γ is the energy separation of the ^2E and the singlet state (sometimes called the tunneling splitting).

Chase[14] has pointed out some interesting changes that occur in the $\{1\bar{1}0\}$ plane angular variation of the EPR spectrum as 3Γ is decreased from its value in the dynamic region. In the dynamic region, the angular variation of the extremes for large random strain is given by Eq. (12). For the $\{110\}$ planes, $l = m$ and therefore at any point in the plane, the outer extremes of the ^2E spectrum occur for $\phi = 0$ or π, i.e., for those sites with $e_\epsilon = 0$. The wavefunctions for the sites with $\phi = 0$ are $\Psi_+ = \Psi_{g\epsilon}$ and $\Psi_- = \Psi_{g\theta}$; for the sites with $\phi = \pi$ we have $\Psi_+ = \Psi_{g\theta}$ and $\Psi_- = -\Psi_{g\epsilon}$. For a d^9 configuration ion, qg_2 is positive, and thus from Eqs. (11) and (12) it is apparent that $\Psi_{g\theta}$ states give rise to the high-field side of the spectrum for orientations between $\vec{H} \parallel [001]$ and $\vec{H} \parallel [111]$ and the low-field side for orientations between $\vec{H} \parallel [111]$ and $\vec{H} \parallel [110]$. The $\Psi_{g\epsilon}$ states produce the opposite side of the spectrum at these orientations. Consider the matrices in Eqs. (15) and (16) where random strain and tunneling are assumed to be the largest perturbations. Let $e_\epsilon = 0$. As the tunneling splitting is decreased from the dynamic region, Ψ_{A1} is only admixed with $\Psi_{g\theta}$, and Ψ_{A2} is only admixed with $\Psi_{g\epsilon}$. The expectation value of the Zeeman interactions for the admixed state with A_1 lowest then contains the term

$$\langle \Psi_{A1} | rV_2 e_\theta | \Psi_{g\theta} \rangle \langle \Psi_{g\theta} | rG_\theta | \Psi_{A1} \rangle / 3\Gamma ,$$

where G_θ is that part of the Zeeman interaction which transforms as the θ component of E, and the result of this term is to broaden and shift the resonance-field position associated with $\Psi_{g\theta}$. For A_2 lower the corresponding term is

$$\langle \Psi_{A2} | -rV_2 e_\theta | \Psi_{g\epsilon} \rangle \langle \Psi_{g\epsilon} | -rG_\theta | \Psi_{A2} \rangle / 3\Gamma ,$$

which results in a similar broadening and shifting of the resonance-field position associated with $\Psi_{g\epsilon}$. In the EPR spectrum due to the ground Kramers's doublet, the resonance-field positions of the "coupled" side of the spectrum are shifted in a manner which results in an increase in the total anisotropy of the angular variation in the $\{110\}$ plane. It should be noted that the side of the spectrum in the $\{1\bar{1}0\}$ plane which is not affected by the selective coupling allows a determination to be made of the spin-Hamiltonian parameters g_1, qg_2, A_1, and qA_2 which is independent of intermediate JT effects.

In order to consider the transition from dynamic to static JT effects, it is convenient to express the matrices [Eqs. (15) and (16)] relative to the vibronic basis functions Ψ_1, Ψ_2, Ψ_3, where[1]

$$\begin{aligned} \Psi_{A1} &= (1/\sqrt{3})(\Psi_1 + \Psi_2 + \Psi_3) , \\ \Psi_{g\theta} &= (1/\sqrt{6})(2\Psi_1 - \Psi_2 - \Psi_3) , \\ \Psi_{g\epsilon} &= (1/\sqrt{2})(\Psi_2 - \Psi_3) , \end{aligned} \tag{18}$$

for A_1 lowest or

$$\begin{aligned} \Psi_{A2} &= (1/\sqrt{3})(\Psi_1 + \Psi_2 + \Psi_3) , \\ \Psi_{g\theta} &= (1/\sqrt{2})(\Psi_3 - \Psi_2) , \\ \Psi_{g\epsilon} &= (1/\sqrt{6})(2\Psi_1 - \Psi_2 - \Psi_3) , \end{aligned} \tag{19}$$

for A_2 lowest. The matrix elements of $\mathcal{H}$ relative to the new basis are then given by the following expressions:

$$\begin{aligned} \mathcal{H}_{11} &= \Gamma + G_1 \mp \tfrac{2}{3}(q - \sqrt{2}r)G_\theta , \\ \mathcal{H}_{22} &= \Gamma + G_1 \mp \tfrac{1}{3}(q - \sqrt{2}r)(-G_\theta + \sqrt{3}G_\epsilon) , \\ \mathcal{H}_{33} &= \Gamma + G_1 \mp \tfrac{1}{3}(q - \sqrt{2}r)(-G_\theta - \sqrt{3}G_\epsilon) , \\ \mathcal{H}_{12} &= \mathcal{H}_{21} = \Gamma \pm \tfrac{1}{6}\sqrt{2}(\sqrt{2}q + r)(G_\theta + \sqrt{3}G_\epsilon) , \\ \mathcal{H}_{13} &= \mathcal{H}_{31} = \Gamma \pm \tfrac{1}{6}\sqrt{2}(\sqrt{2}q + r)(G_\theta - \sqrt{3}G_\epsilon) , \\ \mathcal{H}_{23} &= \mathcal{H}_{32} = \Gamma \pm \tfrac{1}{3}\sqrt{2}(\sqrt{2}q + r)G_\theta , \end{aligned} \tag{20}$$

where $\mathcal{H}_{ij} = \langle \Psi_i | \mathcal{H} | \Psi_j \rangle$ with $i, j = 1, 3$, and the upper signs are appropriate for A_1 lowest and the lower signs for A_2 lowest. The Ψ_1, Ψ_2, and Ψ_3 wave functions have special significance for the case of strong JT coupling. In the strong-coupling limit, the wave functions are given by Born–Oppenheimer products of electronic and vibrational wave functions. If sufficient warping is present so that there is negligible overlap between the vibrational wave functions associated with each distorted configuration, then each of the Ψ_i $(i = 1, 2, 3)$ wave functions corresponds to a vibronic state with a distortion along one of the three cubic axes. In this limit, Ham[1] has shown that $r = -\sqrt{2}q$, so that the diagonal matrix elements of $\mathcal{H}$ become

$$\begin{aligned} \mathcal{H}_{11} &= \Gamma + G_1 \mp 2qG_\theta , \\ \mathcal{H}_{22} &= \Gamma + G_1 \mp q(-G_\theta + \sqrt{3}G_\epsilon) , \end{aligned} \tag{21}$$

$$\mathcal{H}_{33} = \Gamma + G_1 \mp q(-G_\theta - \sqrt{3}\,G_\epsilon)\ ,$$

and all off-diagonal elements equal Γ. If the Zeeman and hyperfine operators in Eq. (8) are substituted into Eq. (21), these matrix elements, which have the same form as the usual axial spin Hamiltonian with unique principal axes along the z, x, and y directions, are as follows:

$$\begin{aligned}
\mathcal{H}_{11} &= \Gamma + g_\parallel \mu_B H_z S_z + g_\perp \mu_B (H_x S_x + H_y S_y) \\
&\quad + A_\parallel S_z I_z + A_\perp (S_x I_x + S_y I_y)\ , \\
\mathcal{H}_{22} &= \Gamma + g_\parallel \mu_B H_x S_x + g_\perp \mu_B (H_z S_z + H_y S_y) \\
&\quad + A_\parallel S_x I_x + A_\perp (S_z I_z + S_y I_y)\ , \\
\mathcal{H}_{33} &= \Gamma + g_\parallel \mu_B H_y S_y + g_\perp \mu_B (H_x S_x + H_z S_z) \\
&\quad + A_\parallel S_y I_y + A_\perp (S_x I_x + S_z I_z)\ ,
\end{aligned} \tag{22}$$

where $g_\parallel = g_1 \mp 2qg_2$; $g_\perp = g_1 \pm qg_2$; $A_\parallel = A_1 \mp 2qA_2$; and $A_\perp = A_1 \pm qA_2$. Again the upper (lower) sign corresponds to the A_1 (A_2) state being lowest. (Note that unfortunately the same A_1, A_2 notation is conventionally used to label both the vibronic excited states and the hyperfine parameters.) When Γ is small compared to the Zeeman interaction, three axially symmetric EPR spectra which are described by Eqs. (22) are observed in the absence of random strain. The effect of random strain is expected to be larger than the Zeeman interaction, however, so that the matrix of strain [Eq. (7)] and tunneling should determine the eigenstates of the system. If the relation $r = -\sqrt{2}q$ is assumed valid, this matrix has the following form with respect to the basis Ψ_1, Ψ_2, and Ψ_3:

$$\begin{pmatrix}
\Gamma \mp \delta\cos\phi/2q & \Gamma & \Gamma \\
\Gamma & \Gamma \pm \delta(\cos\phi - \sqrt{3}\sin\phi)/2q & \Gamma \\
\Gamma & \Gamma & \Gamma \pm \delta(\cos\phi + \sqrt{3}\sin\phi)/2q
\end{pmatrix}\ , \tag{23}$$

where $\delta = 2q|V_2|(e_\theta^2 + e_\epsilon^2)^{1/2}$ is the strain splitting appropriate to the isolated ^2E state,

$$e_\theta = (\delta\cos\phi)/2q|V_2|\ ,$$

$$e_\epsilon = (\delta\sin\phi)/2q|V_2|\ ,$$

and ϕ determines the distribution of strain between θ and ϵ components. For large values of $\delta/3\Gamma$, the eigenstates are essentially the three Kramers' doublets Ψ_1, Ψ_2, and Ψ_3, and the EPR spectrum displays the static JT effect described by Eq. (22). It should be noted that, in the limit $\delta \gg 3\Gamma$, each of the Ψ_i Kramers' doublets becomes the ground state as ϕ is varied in the range $0 \le \phi \le 2\pi$. For a crystal with a distribution of random strain in which all values of ϕ in the range $0 \le \phi \le 2\pi$ are equally likely, only the ground-state Kramers' doublet at each site need be populated in order to have all three distorted configurations simultaneously present in the crystal. Thus, the static JT effect is observed even if $kT \ll 3\Gamma$.

The following discussion will describe the effects on the EPR spectra resulting from intermediate values of $\delta/3\Gamma$ in Eq. (23). In particular, it is important to detail how the EPR spectra for intermediate values of $\delta/3\Gamma$ differ from those characteristic of either the static or dynamic JT effect. In order to predict the effects of intermediate values of $\delta/3\Gamma$, it is necessary to perform a numerical diagonalization of Eq. (23) for a given $\delta/3\Gamma$ value. Since the Zeeman and hyperfine interactions are assumed to be small compared with strain and tunneling, the EPR spectrum can be computed by perturbation theory for each Kramers' doublet resulting from the diagonalization. The formulation in Eq. (23) rather than Eqs. (15) and (16) is more convenient for this purpose due to the diagonal form of the Zeeman and hyperfine operators relative to the Ψ_1, Ψ_2, Ψ_3 basis. Specifically, once the eigenstates $\Phi_i = \sum_{j=1}^{3} C_{ij}\Psi_j$ of Eq. (23) are determined, then (as long as $r = -\sqrt{2}q$) the expectation values of the hyperfine and Zeeman operators $\langle \Phi_i | \mathcal{H} | \Phi_i \rangle$ for each Kramers' doublet are simply and accurately calculated since $\langle \Psi_j | \mathcal{H} | \Psi_k \rangle$ is a diagonal matrix. A calculation of this type was first described by Chase,[14] and we have successfully employed it to describe the EPR spectra of Ag^{2+} in MgO and CaO.[15]

Since little is known about the distribution of random strain in the crystal, some assumptions in this regard must be made in order to calculate the EPR spectrum resulting from the crystal as a whole. In this work the probability $P(\delta)$ of a given site having a random-strain splitting δ was assumed to have a Gaussian distribution about a mean strain $\bar{\delta}$:

$$P(\delta) \propto e^{-(\delta - \bar{\delta})^2/2\sigma^2}\ .$$

A distribution not centered about zero-strain splitting was chosen in order to be consistent with the previous assumption that the random-strain splitting should be considerably larger than the Zeeman interaction. This distribution is also consistent with the observed occurrence of large tetragonal strain in the EPR spectra of many rare-earth and transition-group ions doped into alkaline-

earth oxide crystals.[5,29] A Gaussian linewidth was also assumed for the EPR transitions associated with a given site in the crystal (due to spin-spin interactions, lifetime effects, etc.). Thus it was possible to vary the EPR line shape associated with the bulk crystal by changing either the width of the component EPR transitions or the width of the distribution of random-strain splittings (σ). For simplicity, however, σ was set equal to $\bar{\delta}$ and the line shape varied by changing the width of the component transitions. Once δ was chosen from this distribution, the matrix in Eq. (23) was diagonalized and the EPR transitions were computed for a fixed number (≈ 200) of ϕ values uniformly distributed over the region $0 \leq \phi \leq 2\pi$. For a given choice of δ and ϕ, the EPR spectrum for each Kramers' doublet resulting from the diagonalization was weighted by the Boltzmann factor appropriate to the assumed temperature, and the contributions to the total EPR spectrum were then summed over the values of ϕ and weighted by the distribution of δ. Only the usual allowed ($\Delta M_S = \pm 1$, $\Delta M_I = 0$) EPR transitions were considered, and the relation $r = -\sqrt{2}q$ was also assumed.

Figure 1 shows the type of line-shape changes predicted by the technique described above for a typical EPR absorption spectrum as a function of $\bar{\delta}/3\Gamma$. The spectra in Fig. 1 were computed with the assumption that A_2 is lowest and with $\vec{H} \parallel [001]$, $g_1 = 2.0$, $qg_2 = 0.05$, and $kT \ll 3\Gamma$. No hyperfine structure was included. As $\bar{\delta}/3\Gamma$ is increased from 0.01, the low-field extreme is broadened and then shifted to lower field. This shift increases with increasing $\bar{\delta}/3\Gamma$ until $\bar{\delta}/3\Gamma \simeq 2$ where the rate of change in resonance-field position becomes relatively small. Both sides of the spectrum become narrower as $\bar{\delta}/3\Gamma$ further increases to the static limit $\bar{\delta} \gg 3\Gamma$. The effective g value of the low-field side is shifted from $g = g_1 + qg_2$ at the dynamic limit ($\bar{\delta}/3\Gamma < 0.1$) to $g = g_1 + 2qg_2$ at the static limit ($\bar{\delta}/3\Gamma > 5$). Since the individual absorption spectra are not normalized relative to each other, the changes in the spectral line intensities would be much greater than those shown in the figure. Figure 2 shows the computed angular variations in a {110} plane of the absorption peaks for the same $\bar{\delta}/3\Gamma$ values used in Fig. 1. As noted above, only one side of the spectrum in this plane is shifted by strain coupling to the A_2 level.

In addition to the calculated changes in the angular variation, shown in Fig. 2, significant changes in the line shape with varying $\bar{\delta}/3\Gamma$ are predicted when $\vec{H}$ is parallel to one of the ⟨111⟩ directions. Figure 3 shows the type of changes that occur in the $\vec{H} \parallel [111]$ line shape for three values of $\bar{\delta}/3\Gamma$ in the intermediate-coupling region. The top trace shows the EPR absorption line, and the corresponding first derivative is shown below. These lines were computed for $\nu_e = 23.0$ GHz, $g_1 = 2.0$, and $qg_2 = 0.05$ with an A_2 level assumed lower. A Gaussian linewidth for each spin transition was assumed. For $\bar{\delta}/3\Gamma = 0.33$, the maximum absorption intensity occurs near the high-field side of the line corresponding to a system more characteristic of the dynamic JT effect. This distortion in the line shape is a reflection of the different g values for the dy-

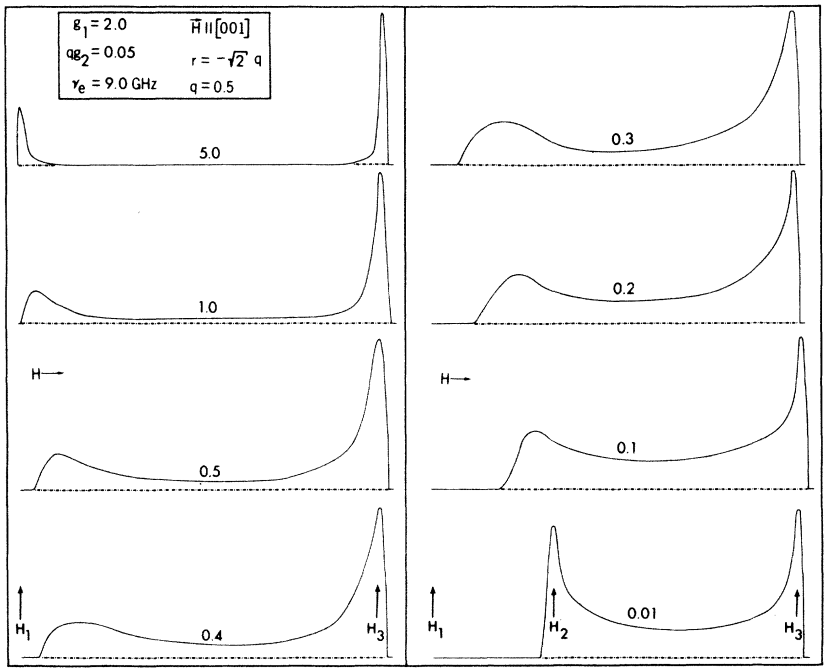

FIG. 1. EPR absorption line shapes calculated as a function of $\bar{\delta}/3\Gamma$. The appropriate $\bar{\delta}/3\Gamma$ values are shown over each spectrum. An A_2 level is assumed to be the lowest vibronic singlet. The field positions H_1, H_2, and H_3 are given by $H_1 = h\nu(g_1 + 2qg_2)\mu_B$, $H_2 = h\nu/(g_1 + qg_2)\mu_B$, and $H_3 = h\nu/(g_1 - qg_2)\mu_B$.

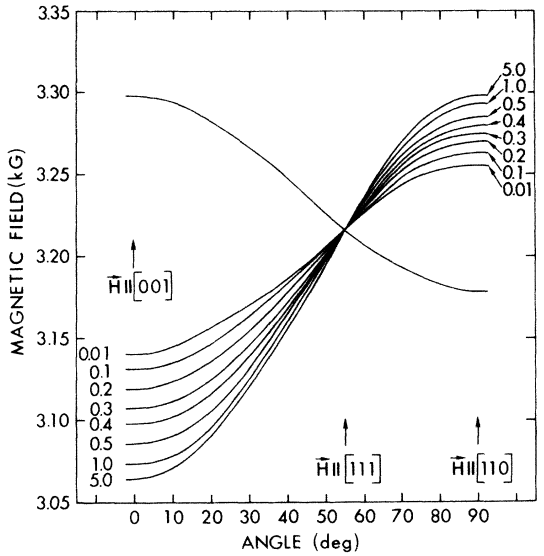

FIG. 2. Dependence of the $(1\bar{1}0)$ plane angular variation on $\bar{\delta}/3\Gamma$. The $\bar{\delta}/3\Gamma$ values associated with each curve correspond to those used in Fig. 1. The A_2 level is the lowest singlet. The resonance-field position of the extreme on one side of the spectrum is independent of $\bar{\delta}/3\Gamma$ in this plane.

namic and static cases with $\vec{H} \| \langle 111 \rangle$. The g value for a purely dynamic case with $\vec{H} \| \langle 111 \rangle$ is

$$g = [g_1^2 + \tfrac{1}{2}(qg_2)^2]^{1/2} ,$$

while for a pure static case the corresponding relation is

$$g = [g_1^2 + 2(qg_2)^2]^{1/2} .$$

These g values differ slightly in the usual case where $|qg_2| \ll g_1$, and for a system with intermediate JT coupling present, the observed resonance components are distributed between these limits. The "dynamic" portion of the resonance absorption therefore occurs at the high-field side of the line. For $\bar{\delta}/3\Gamma = 1.0$, the spectrum in Fig. 3 shows an almost equal distribution between "static" and "dynamic" resonance positions, while for $\bar{\delta}/3\Gamma = 2.0$, the "static" line shape is seen to predominate. A distortion in the line shape with $\vec{H} \| \langle 111 \rangle$ was observed for Ag^{2+} in CaO[15] and, as will be shown below, has also been observed for Cu^{2+} in both CaO and MgO.[18]

Although the dynamic and static effects are only the two limiting cases of a continuous range of JT coupling effects at low temperature, we have shown that[15,30] the changes produced in the observed EPR spectrum by varying the JT coupling strength are striking. In classifying the observed changes, we have employed the following broad (and somewhat overlapping) categories:

(a) "Pure dynamic" for the case of a ^2E state in cubic symmetry which is sufficiently isolated from the A_1 or A_2 levels so that no effects of coupling to these singlets are observed in the EPR spectra other than perhaps a slight broadening of one side of the spectrum $(\bar{\delta}/3\Gamma < 0.1)$.

(b) "Quasidynamic" for those cases where effects of coupling to the singlet levels are observed in the angular variation but three distinct tetragonal-symmetry spectra are *not* observed $(0.1 < \bar{\delta}/3\Gamma < 0.8)$.

(c) "Quasistatic" for those cases where three

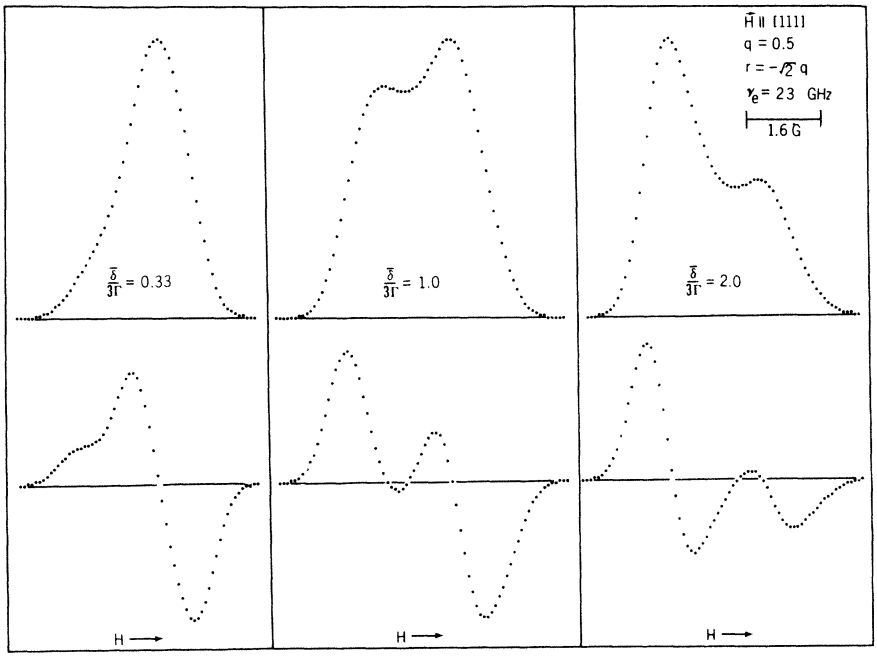

FIG. 3. Calculated EPR line shapes at $\vec{H} \| [111]$ for three $\bar{\delta}/3\Gamma$ values in the intermediate JT coupling region. The absorption line shape is placed above its respective first derivative.

tetragonal-symmetry spectra are observed, but the ratio $\bar{\delta}/3\Gamma$ is sufficiently small to produce significant line-shape distortion ($0.3 < \bar{\delta}/3\Gamma < 5$).

(d) "Pure static" for those cases where three distinct tetragonal-symmetry spectra are observed and the ratio $\bar{\delta}/3\Gamma$ is sufficiently large so that the typical symmetric EPR line shapes are observed ($\bar{\delta}/3\Gamma > 5$).

III. SUMMARY OF PREVIOUS EPR INVESTIGATIONS OF MgO:Cu^{2+} AND CaO:Cu^{2+}

The EPR spectra of Cu^{2+} in MgO and CaO single crystals have been the subject of several previous investigations. Orton *et al.*[31] first studied MgO:Cu^{2+} and found that the Cu^{2+} EPR spectrum was isotropic at temperatures above 4 K but that at 1.2 K the isotropic spectrum was replaced by an anisotropic spectrum. The anisotropic spectrum was not analyzed in detail by Orton *et al.* but its existence was attributed to the JT effect. Low and Suss[5] found similar results for the temperature dependence of the CaO:Cu^{2+} EPR spectrum and measured the transition temperature to be about 1.7 K. The low-temperature CaO:Cu^{2+} spectrum was described by Low and Suss as corresponding to three inequivalent ions per unit cell with tetragonal distortions along the cubic axes and with $g_{\parallel}$ apparently less than $g_{\perp}$. Using the theoretical analysis of O'Brien,[24] they concluded that in CaO:Cu^{2+} a compression of the CuO_6 octahedron was stabilized at low temperature.

Coffman *et al.*[32,33] subsequently studied the EPR spectra of both MgO:Cu^{2+} and CaO:Cu^{2+} and found that both spectra were appropriate to one inequivalent ion per unit cell and that the observed X-band angular variations were not consistent with the axial site symmetry expected for the static JT effect. Using the tunneling model of Bersuker[22,23] and O'Brien,[24] Coffman[32] determined that the angular variation of the MgO:Cu^{2+} spectrum was consistent with that expected for a tunneling quartet (i.e., an isolated ground ^2E vibronic ground state plus Kramers' degeneracy, which is produced by strong JT coupling with $q \simeq \frac{1}{2}$). From studying the CaO:Cu^{2+} (100)-plane angular variation, Coffman *et al.*[33] found that for this system an appreciable interaction must occur between the ground vibronic doublet and the excited singlet and that this interaction was appropriate to a tunneling splitting of $3\Gamma = 0.006$ cm^{-1}. Unfortunately, neither the CaO:Cu^{2+} nor MgO:Cu^{2+} analysis included random strain effects which were later shown to be of great significance in JT systems. Also, both investigations were handicapped since a large part of the total Cu^{2+} angular variation could not be observed due either to large linewidth increases near $\vec{H} \parallel \langle 100 \rangle$ or to the presence of overlapping EPR spectra from other impurity ions. In the present work, the intensity of the Cu^{2+} EPR spectrum in both hosts was sufficient to eliminate most of these difficulties.

Other experimental EPR investigations and related analyses of MgO:Cu^{2+} and CaO:Cu^{2+} have been performed,[34-36] but in each case the effects of random strain were ignored or were assumed to involve only the ground vibronic doublet.

IV. RESULTS AND DISCUSSION

In the present study, Cu-doped MgO and CaO single crystals were grown by an arc-fusion technique described previously.[37] The dopant was added to the melt in the form of CuO. The resulting MgO crystals were colorless in appearance while the CaO:Cu crystals were yellow-green. The EPR spectra were observed in the "as-grown" crystals using 9- and 24-GHz homodyne EPR spectrometers both of which permitted *in situ* orientation of the single-crystal sample. Unless otherwise indicated, all observations discussed below relate to the 9-GHz spectra.

The EPR spectrum observed for Cu^{2+} in both CaO and MgO at 77 K consisted of two sets of four partially overlapping hyperfine lines. The fourfold multiplicity of each set of lines is due to the two naturally occurring Cu isotopes, ^{63}Cu and ^{65}Cu, both of which have a nuclear spin $I = \frac{3}{2}$. The two sets of four lines are partially superimposed as a result of the similarity of the nuclear moments of ^{63}Cu and ^{65}Cu ($\mu = +2.223\mu_N$ for ^{63}Cu and $\mu = +2.382\mu_N$ for ^{65}Cu) combined with the width of the component resonance lines. The magnetic-field positions of the centers of the lines were independent of the orientation of the applied magnetic field relative to the symmetry axes of the host crystal at 77 K; however, anisotropy in the width of the resonance lines was observed at this temperature. The lines were narrowest in both hosts for $\vec{H} \parallel \langle 111 \rangle$ and broadened as the applied magnetic field was rotated away from that orientation. For CaO:Cu^{2+} at 9 GHz, the lines were 3 G wide at $\vec{H} \parallel \langle 111 \rangle$ allowing a 1–2-G resolution of the ^{63}Cu and ^{65}Cu hyperfine lines for the transitions with $|M_I| = \frac{3}{2}$ (Fig. 4). At 77 K the linewidths for Cu^{2+} in MgO with $\vec{H} \parallel \langle 111 \rangle$ were ≈ 7 G. Measurements at 9 GHz of the spectra for $\vec{H} \parallel \langle 111 \rangle$ for both hosts were fit by the spin Hamiltonian $\mathcal{H} = g\mu_B \vec{H} \cdot \vec{S} + A\vec{I} \cdot \vec{S}$ with the parameters given in Table I. These parameters are in agreement with those previously reported.[5,31,32]

At 1.3 K the Cu^{2+} EPR spectra in both hosts were anisotropic and, except for magnetic-field orientations within a few degrees of $\vec{H} \parallel \langle 111 \rangle$, consisted of four strain-broadened hyperfine lines with anisotropic and asymmetric line shapes. The partial resolution of the ^{63}Cu and ^{65}Cu isotopes

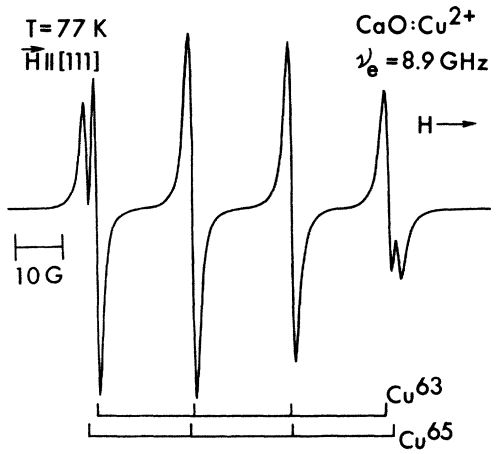

FIG. 4. EPR spectrum of Cu^{2+} in CaO observed with $\vec{H} \parallel [111]$ at 77 K. The line positions are isotropic at this temperature but some anisotropy in linewidth is present. Partial resolution of the hyperfine structure of the two naturally occurring Cu isotopes, ^{63}Cu and ^{65}Cu, is present.

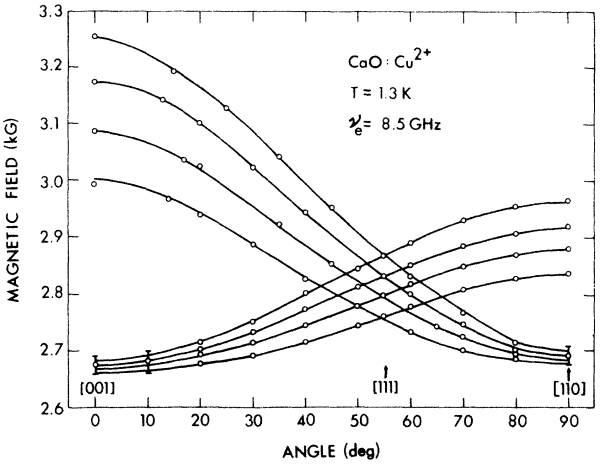

FIG. 5. Calculated and observed angular dependence of the low-temperature $CaO : Cu^{2+}$ EPR spectrum in the $(1\bar{1}0)$ plane. The solid curves represent the angular variation calculated using the effective Hamiltonian parameters listed in Table II and a value of 0.67 for $\bar{\delta}/3\Gamma$. The open circles represent the experimentally determined resonance-field positions of the extremes of each of the four strain-broadened lines. (The ^{63}Cu and ^{65}Cu isotopes could not be resolved at 1.3 K.) The "hyperfine structure" of the low-field extremes near $\vec{H} \parallel [001]$ and $\vec{H} \parallel [110]$ cannot be resolved experimentally.

which was evident at 77 K (see Fig. 4) was not present at 1.3 K, and both anisotropic extremes of each of the four hyperfine lines were composed of unresolved hyperfine extremes of the two Cu isotopes. The angular dependence of the EPR spectrum obtained at 9 GHz for Cu^{2+} in both hosts was determined for magnetic field orientations throughout the entire $(1\bar{1}0)$ plane. These angular variations are shown in Figs. 5 and 6. In each host, the two sets of anisotropic extremes were essentially superimposed at $\vec{H} \parallel \langle 111 \rangle$, and the extremes split up, decreased in intensity, and rapidly broadened as $\vec{H}$ was rotated away from a $\langle 111 \rangle$ direction in a $\{110\}$ plane. As the magnetic-field orientation approached $\vec{H} \parallel \langle 001 \rangle$, the extremes at high field for $CaO : Cu^{2+}$ and at low field for $MgO : Cu^{2+}$ became difficult to observe due to broad linewidths and low intensities. As indicated in Fig. 5, for $CaO : Cu^{2+}$ the separation of the low-field extremes of each hyperfine component near the orientations $\vec{H} \parallel \langle 100 \rangle$ and $\vec{H} \parallel \langle 110 \rangle$ was sufficiently small to prevent resolution of the individual hyperfine extremes.

TABLE I. Spin-Hamiltonian parameters for Cu^{2+} in MgO and CaO at 77 K.

Host	g	A (10^{-4} cm^{-1})	Ref.
MgO	2.1933(8)	18.7(8)	a
MgO	2.192(1)	19.0	b
MgO	2.190(2)	19(1)	c
CaO	2.2205(6)	21.8(4)	a
CaO	2.2201(6)	21.6(3)	d

[a]This work.
[b]Reference 32.
[c]Reference 31.
[d]Reference 5.

In the 24-GHz EPR spectra of both hosts, the effects of line broadening as a function of the applied magnetic field were more severe, and the complete $(1\bar{1}0)$ plane angular variation could not be obtained for either host at this frequency.

For Cu^{2+} in both CaO and MgO the number of anisotropic components observed at 1.3 K, the observed asymmetric line shapes, and, to some extent, the observed angular dependences are characteristic of the strain-broadened EPR lines produced by the dynamic JT effect. There are, however, some very significant discrepancies between the observed EPR spectra and the spectrum expected for an isolated ^2E vibronic level. For $CaO : Cu^{2+}$ the four extremes of the spectrum that appear at low field near $\vec{H} \parallel [001]$ and at high field near $\vec{H} \parallel [110]$ are sharper and more intense than the other extremes. For $MgO : Cu^{2+}$ the opposite is true (i.e., it is the extremes that are at high field near $\vec{H} \parallel [001]$ and at low field near $\vec{H} \parallel [110]$ that are sharper). For $MgO : Cu^{2+}$, however, the difference between the high- and low-field extremes is much less than that observed for $CaO : Cu^{2+}$. As discussed in Sec. II, this type of selective line broadening in a $\{110\}$ plane can be attributed to coupling of the ^2E ground state to the next excited vibronic singlet via the random strain interaction. The particular side of the spectrum affected by this broadening indicates that the coupled singlet level is the A_1 level for $CaO : Cu^{2+}$ and the A_2 level for

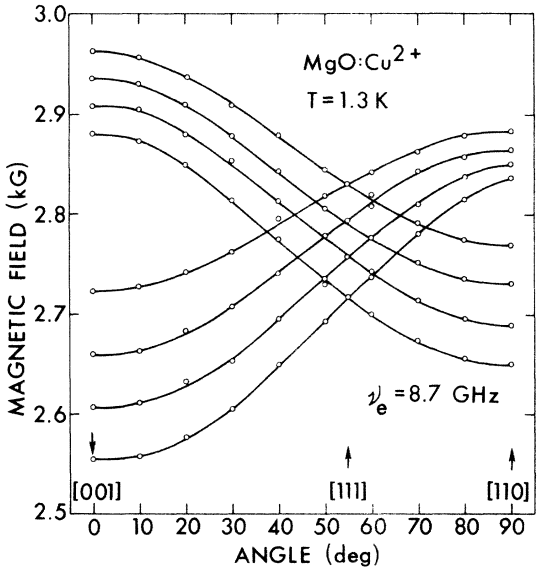

FIG. 6. Observed angular dependence of the low-temperature MgO : Cu^{2+} EPR spectrum in the $(1\bar{1}0)$ plane. Here the solid curves represent an approximate fit to the experimental data points and are not the calculated angular variations as shown in Fig. 5.

MgO : Cu^{2+}. (In the case of MgO : Cu^{2+}, this observation was previously made by Ham[1] from unpublished data of Geschwind and Brya. Low and Suss[5] made an equivalent observation for CaO : Cu^{2+} although, in this case, they classified the JT effect as static.)

Additional departures from purely dynamic JT effects are observed in the {110} plane angular variations in both hosts. For CaO : Cu^{2+} and MgO : Cu^{2+}, it was found that both sides of the {110} plane angular variations could not be simultaneously fit to Ham's effective Hamiltonian for an isolated ^2E state with large random strains [Eq. (5)]. When the sharp extremes of the $(1\bar{1}0)$ plane angular dependence were used to determine the effective spin-Hamiltonian parameters, it was found that for both CaO : Cu^{2+} and MgO : Cu^{2+} the observed resonance fields for the broad extremes were shifted to magnetic-field values further displaced from the field position for $\vec{H} \parallel \langle 111 \rangle$ than those calculated from the solutions to Eq. (5). The shift for CaO : Cu^{2+} was much larger than for MgO : Cu^{2+}. This shift in magnetic-field position is also indicative of the coupling to an excited vibronic state that is characteristic of intermediate JT effects.

The computer technique described in Sec. II was used to determine whether the presence of random strain coupling to an excited A_1 vibronic singlet would account for the observed CaO : Cu^{2+} {110} plane angular variation. Using the effective spin-Hamiltonian parameters calculated from the sharp extremes of the CaO : Cu^{2+} spectrum (plus the assumption valid for strong JT coupling that $q = 0.5$), the complete 1.3-K CaO : Cu^{2+} spectrum was calculated for different magnetic-field orientations in a $(1\bar{1}0)$ plane. Agreement between the computed and observed EPR spectrum was found for all orientations in the plane when $\bar{\delta}/3\Gamma = 0.67$. The solid curves in Fig. 5 represent the computed angular variation, and it is apparent that the agreement is good for both the Zeeman and hyperfine interactions. The effective Hamiltonian parameters are given in Table II.

The computed angular variation in the (001) plane for CaO : Cu^{2+} with $\bar{\delta}/3\Gamma = 0.67$ is shown in Fig. 7. In addition to the two sets of hyperfine extremes which were present in the (110) plane, an additional four-component structure with low intensity was predicted by the computer. This additional structure is indicated in Fig. 7 by the dashed curves; the computed positions near $\vec{H} \parallel \langle 100 \rangle$ could not be determined due to overlap with the more intense group of superimposed extremes at low field. It is interesting to note that for $\vec{H} \parallel [110]$ the high-field extremes of the larger hyperfine lines (solid curves) do not quite superimpose with the additional weaker structure (dashed curves). The presence of this additional structure was also indicated in the computed spectra in the $(1\bar{1}0)$ plane at orientations between $\vec{H} \parallel [111]$ and $\vec{H} \parallel [110]$. In the $(1\bar{1}0)$ plane, this structure took the form of weak "satellites" at a slightly lower field from the second, third, and fourth hyperfine extremes (counting from high field). Attempts to observe these additional lines experimentally did not yield conclusive results in either plane due to the low intensity coupled with the effects of line broadening as a function of orientation and the obscuring effect of overlapping spectra from other impurities (principally Mn^{2+}). Experimentally determined resonance-field positions for the larger extremes with $\vec{H} \parallel [100]$ and $\vec{H} \parallel [110]$ are shown in Fig. 7 by solid circles. The observed (001) plane angular variation at intermediate-field orientations was difficult to obtain accurately due to the other impurity-ion spectra. However, agreement between the computed and experimental angular variation was achieved within experimental error. Since the presence of three sets of "hyperfine" structure is predicted by the computer calculation, but is not verified experimentally, the CaO : Cu^{2+} EPR spectra should be classified (according to the terms of the discussion in Sec. II) as being in the overlapping region between the quasidynamic and quasistatic cases.

The presence of intermediate JT coupling in the CaO : Cu^{2+} EPR spectra is also evident in the line shapes observed with $\vec{H} \parallel \langle 111 \rangle$. The EPR spectrum observed at 1.3 K for CaO : Cu^{2+} is shown at the top of Fig. 8 for $\vec{H} \parallel [111]$. The departure from the ex-

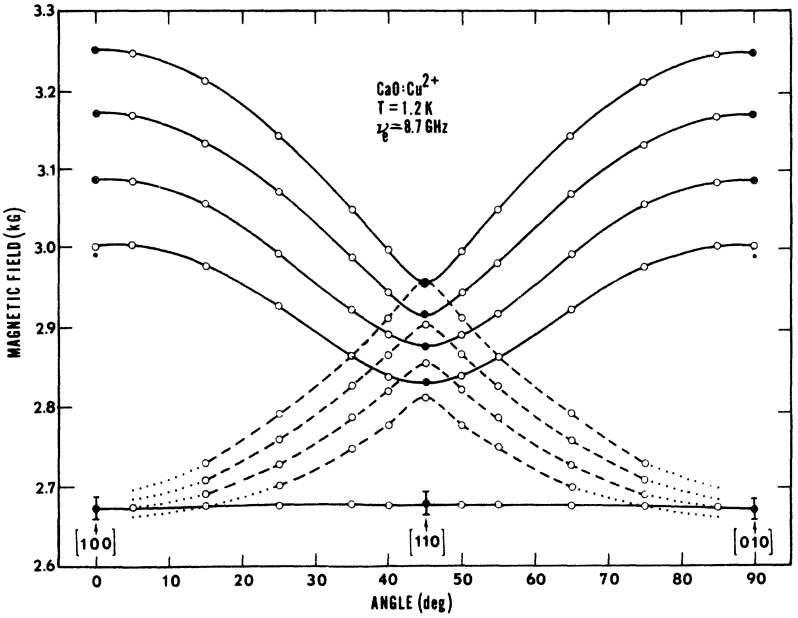

FIG. 7. Calculated $CaO:Cu^{2+}$ angular dependence in the (001) plane with strain coupling to an excited A_1 vibronic singlet. A value of 0.67 was used for $\bar{\delta}/3\Gamma$. Observed resonance field positions of the extremes at $\vec{H} \| [100]$ and $\vec{H} \| [110]$ are indicated by solid circles. The dashed curves show the calculated angular variation of the structure whose intensity is predicted to be very weak relative to the components whose angular variation is indicated by the solid curves. This structure was too weak to be observed experimentally.

pected four-line hyperfine of pattern of Fig. 4 is striking and is not due to misalignment of the crystal or to resolution of the Cu^{2+} isotopes. Unusual EPR line shapes were observed previously for the low-temperature $CaO:Ag^{2+}$ EPR spectrum with $\vec{H} \| [111]$ and were shown to result from intermediate JT coupling effects.[15] With the same computer technique described above, the $CaO:Cu^{2+}$ EPR spectrum was calculated for $\vec{H} \| [111]$ using the same spin-Hamiltonian parameters and $\bar{\delta}/3\Gamma$ value that successfully duplicated the angular variation of the high-intensity extremes in the $(0\bar{1}1)$ plane. A Gaussian linewidth for each transition was assumed and q was fixed at 0.5. The presence of two distinct Cu^{2+} isotopes was ignored due to the width of the observed resonance lines. The resulting computed EPR spectrum is shown at the bottom of Fig. 8. All features of the observed spectrum are duplicated in the calculated spectrum with the exception of two small lines (denoted by asterisks) on either side of the most intense (clipped) line. This small additional structure is believed to be due to forbidden hyperfine transitions induced by a nuclear-quadrupole interaction.[29] The successful duplication of the unusual line shapes for $\vec{H} \| [111]$ provides a convincing demonstration of the effects of intermediate JT coupling in the Cu^{2+} ground state in CaO.

The $CaO:Cu^{2+}$ spectrum at 24 GHz (Fig. 9) with $\vec{H} \| \langle 111 \rangle$ exhibited noticeably different line shapes from those observed at 9 GHz. A similar change in line shape was observed in the EPR spectrum of $CaO:Ag^{2+}$ with $\vec{H} \| \langle 111 \rangle$ between 9 and 24 GHz.[15,17] This change with increasing field strength indicates that the Zeeman interaction at 24 GHz is not longer negligible relative to the strain and tunneling splitting. The calculation of the effects of an appreciable Zeeman interaction by including the Zeeman interaction in Eq. (23) necessitates a repeated diagonalization of a 6×6 matrix since the Kramers' degeneracy is removed. If the basis states of the matrices in Eqs. (15) and (16) are employed and the coordinate system is rotated so that $\vec{H} \| z$, then the Zeeman terms off-diagonal in

TABLE II. Effective Hamiltonian parameters for Cu^{2+} in MgO and CaO determined at a temperature of 1.3 K.

Host	$\bar{\delta}/3\Gamma$	g_1	qg_2	A_1 (10^{-4} cm^{-1})	qA_2 (10^{-4} cm^{-1})	Ref.
CaO	0.67	2.2211(7)	+0.122(1)	±31.2(8)	∓24(2)	a
MgO	0.12[b]	2.1924(7)	+0.108(1)	±37.8(8)	±11(2)	a
	...	2.195	+0.108	...	...	c

[a]This work. Values were determined from the 8.5-GHz spectrum.
[b]Note qualification on this measurement as made in text.
[c]Calculated by F. S. Ham from data in Ref. 32 and reported in Ref. 1.

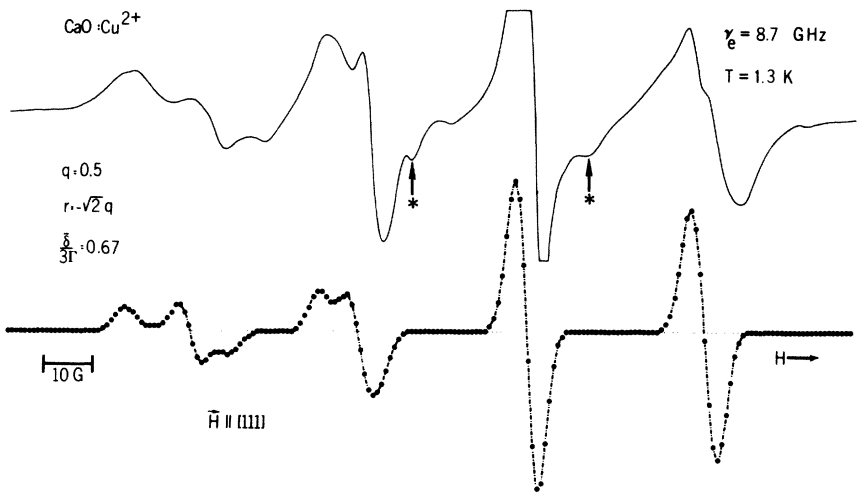

FIG. 8. Top: The observed first derivative presentation of the low-temperature CaO : Cu^{2+} EPR spectrum with $\vec{H} \parallel [111]$ and $\nu_e \simeq 8.7$ GHz. Bottom: The computer generated CaO : Cu^{2+} EPR spectrum for the same orientation assuming strain coupling to an excited A_1 singlet with $\bar{\delta}/3\Gamma = 0.67$. The relatively weak structure denoted by asterisks is believed to be associated with "forbidden" $\Delta M_I = \pm 1$ transitions which arise as the result of a quadrupole interaction of the type discussed in Ref. 28. This quadrupole interaction was not included in the calculation of the line shape.

spin are small ($\approx g_2\nu/g_1$) relative to the diagonal terms ($\approx \frac{1}{2}\nu$). It is then sufficiently accurate to numerically diagonalize the 3×3 matrices which are diagonal in the spin and to account for the off-diagonal terms by second-order perturbation corrections to the energy levels. This approach was successfully used to describe the CaO : Ag^{2+} $\vec{H} \parallel [111]$ line shapes at both frequencies to distinguish the values of $\bar{\delta}$ and 3Γ ($3\Gamma = 3.9$ cm^{-1}, $\bar{\delta} = 4.7$ cm^{-1}).[17] In the case of CaO : Cu^{2+}, the spectra observed at 24 GHz with $\vec{H} \parallel [111]$ were not accurately described since the perturbation expressions for the hyperfine interaction in Eqs. (15) and (16) require that $|qA_2| \ll A_1$. This relation is satisfied for CaO : Ag^{2+} but not for CaO : Cu^{2+}. We have found, however, that with $\bar{\delta}/3\Gamma = 0.67$, a tunneling splitting of $3\Gamma \simeq 3$ cm^{-1} is sufficiently small to produce the type of changes seen between the 24- and 9-GHz CaO : Cu^{2+} spectra. Therefore, at 9 GHz the Zeeman interaction (0.3 cm^{-1}) in CaO : Cu^{2+} has a negligible effect on the diagonalization of Eq. (23).

The present interpretation of the CaO : Cu^{2+} spectrum has been recently substantiated by the Raman-scattering results of Guha and Chase on CaO : Cu^{2+} crystals supplied by us.[38] They have identified the energies and probable symmetries for the five lowest vibronic levels with the lowest excited levels occurring at energies of 4 and 26 cm^{-1}. Based on our EPR results, these energies should correspond to the A_1 and A_2 levels, respectively. This result fixes 3Γ at 4 cm^{-1} which compares favorably with our estimate of ≈ 3 cm^{-1}. From our value of 0.67 for $\bar{\delta}/3\Gamma$ and the value of 4 cm^{-1} for 3Γ we can determine a value of 2.7 cm^{-1} for $\bar{\delta}$.

Although we have observed the intermediate JT coupling effects in the CaO : Cu^{2+} spectrum to be more characteristic of the dynamic than the static JT effect, the possibility exists that in other CaO : Cu^{2+} crystals the random strain will be larger and that JT effects will be observed which are more characteristic of the static effect. Indeed, in the initial study of the CaO : Cu^{2+} spectrum, the JT effect was classified as static.[5] In the present study, the samples used were selected from a large fused mass of CaO : Cu crystals on the basis of their optical clarity and perfection. It is conceivable that crystals of lower over-all quality or those grown by another technique (e.g., flux growth) may have larger random strains. We intend to investigate this possible sample dependence at a later date.

Intermediate Jahn-Teller coupling effects are also clearly evident in the EPR spectrum of Cu^{2+} in MgO, however, the details of the spectrum were not adequately described by a calculation similar to that used for the case of Cu^{2+} in CaO. The inclusion of a ${}^2E$-A_2 coupling via random strains could duplicate the observed $(1\bar{1}0)$ plane angular

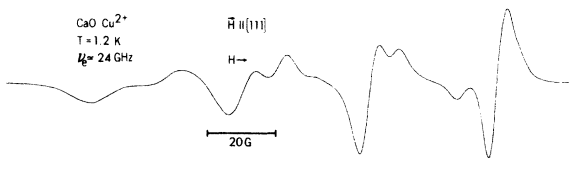

FIG. 9. Low-temperature CaO : Cu^{2+} EPR spectrum observed at 24 GHz with $\vec{H} \parallel [111]$. The difference in line shape between this figure and that shown in Fig. 8 is due to a change in the strength of the Zeeman interaction relative to the random strain and tunneling.

variation of the Zeeman interaction. A value of $\bar{\delta}/3\Gamma = 0.12$ was required along with the effective Hamiltonian parameters determined from the sharper extremes of the spectrum. These effective Hamiltonian parameters are given in Table II. Again $q = 0.5$ was assumed. The angular variation of the hyperfine structure for the broad extremes, however, was not accurately described by this calculation (e.g., at $\vec{H} \parallel [110]$ the broad extreme "hyperfine" separation was approximately twice that actually observed). Also, the asymmetric EPR line shapes observed at 1.3 K for Cu^{2+} in MgO with $\vec{H} \parallel [111]$ (see Fig. 10) could not be accounted for by strain coupling to an excited A_2 singlet with $\bar{\delta}/3\Gamma = 0.12$. In contrast to the case of MgO: Cu^{2+}, the MgO: Ag^{2+} spectrum was completely described with $\bar{\delta}/3\Gamma = 0.13$ and had symmetric EPR line shapes for $\vec{H} \parallel [111]$. Considerably larger values of $\bar{\delta}/3\Gamma$ would be required to explain the MgO: Cu^{2+} line shapes.

Based on the cumulative evidence, we believe that the following explanation can account for the unexpected MgO: Cu^{2+} line shapes with $\vec{H} \parallel [111]$ and for the failure to fit the MgO: Cu^{2+} hyperfine angular variation. For Cu^{2+} in CaO we have shown that the A_1 level is the first excited vibronic state, whereas the A_2 level appears to be the first excited state for Cu^{2+} in MgO. Thus, a crossover of the A_1 and A_2 levels occurs in changing the host from CaO to MgO. It is therefore possible that the energy difference between the A_1 and A_2 levels is not large in the case of MgO: Cu^{2+}. With only linear JT coupling present, the A_1 and A_2 levels are degenerate; and, if additional "warping" terms are small, the A_1 and A_2 levels are closely spaced in energy. If large linear JT coupling and small "warping" terms are present in MgO: Cu^{2+}, random strains could couple both the A_1 and the A_2 levels to the ^2E ground state. In that case, the effect on the low-temperature EPR spectrum would be to increase the anisotropy of each side of the strain-broadened ^2E resonance spectrum. These effects would be difficult to distinguish from the EPR spectrum of an isolated ^2E state which simply had a larger anisotropic Zeeman interaction. If the A_1 and A_2 levels are closely spaced in the MgO: Cu^{2+} system, then the value $\bar{\delta}/3\Gamma = 0.12$ quoted to fit the Zeeman angular variation is indirectly related only to the difference in strain coupling between the two excited vibronic singlets. Two values of this ratio (one for each tunneling splitting and both larger than 0.12) would be necessary to account for all of the observed features of the Cu^{2+} spectrum in MgO. Anisotropic effective Hamiltonian parameters smaller than those given in Table II would also result from this explanation. As mentioned above, larger values of $\bar{\delta}/3\Gamma$ are also necessary to explain the MgO: Cu^{2+} EPR line shapes with $\vec{H} \parallel [111]$. An analysis of the MgO: Cu^{2+} EPR spectrum with a model including strain coupling to both A_1 and A_2 levels would be difficult due to the large number of undetermined parameters (i.e., there is no side of the spectrum unaffected by random strain coupling that one can use to determine the effective Hamiltonian parameters). Therefore such a calculation has not been attempted here. The MgO: Cu^{2+} effective Hamiltonian parameters given here would, however, serve as a useful starting point in such an analysis.

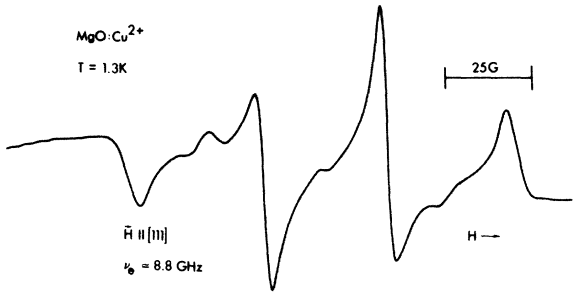

FIG. 10. Low-temperature EPR spectrum of Cu^{2+} in MgO observed with $\vec{H} \parallel [111]$.

The assumption that $q = 0.5$ should be further amplified. Guha and Chase[38] have estimated that $\hbar\omega$ is approximately 300–350 cm^{-1} and E_{JT} is about 6000 cm^{-1} for CaO: Cu^{2+}. Thus, $E_{JT}/\hbar\omega$ is approximately 20 for CaO: Cu^{2+}. The corresponding ratio for MgO: Cu^{2+} has not been determined; however, values for the tunneling splitting for MgO: Ag^{2+}, CaO: Ag^{2+}, and CaO: Cu^{2+} have been previously reported to be 4.8, 3.9, and 4 cm^{-1}, respectively.[15,17,38] These values suggest that 3Γ for MgO: Cu^{2+} should be on the order of 4–5 cm^{-1}. The presence of an isotropic spectrum at 4.2 K is additional evidence that $3\Gamma \leq 10$ cm^{-1} in this material. For MgO: Cu^{2+} (with assumed linear JT coupling) we have the result

$$E_{JT}/\hbar\omega = \hbar\omega/2(3\Gamma) \simeq 40 \tag{24}$$

when the TO-mode frequency in MgO of 393 cm^{-1} is used for $\hbar\omega$. For large linear JT coupling

$$q \simeq \tfrac{1}{2}[1 + (\hbar\omega/4E_{JT})^2], \tag{25}$$

and we should have $q \simeq \frac{1}{2}$ for Cu^{2+} in both hosts. The warping terms should have a negligible effect on this estimate. An approximate value for q can also be calculated from the measured g values if first-order crystal-field theory is assumed to be accurate. In this case we have the following relations[39]:

$$g_1 = g_e - 4\lambda/\Delta\,, \tag{26}$$

$$g_2 = -4\lambda/\Delta\,, \tag{27}$$

where g_e is the free-electron g value, λ is the

spin-orbit-coupling constant, and Δ is the divalent copper ^2E-$^2T_2$ crystal-field splitting. Values of g_2 determined in this manner are 0.190 and 0.219 for MgO and CaO, respectively. These values of g_2 and the measured qg_2 values are used then to obtain $q = 0.568$ and $q = 0.557$ for MgO and CaO, respectively. The q value for MgO: Cu^{2+} must, of course, be considered to be very tentative in the absence of a complete explanation of the MgO: Cu^{2+} EPR spectrum. Since the validity of Eqs. (26) and (27) is affected by covalent bonding, we feel that $q \simeq 0.5$ is the most acceptable estimate for both hosts. The determination that $q \simeq 0.5$ does not support recently published theoretical calculations (employing coupling to more than one vibrational mode) which indicate that q may be substantially smaller than 0.484 for a ^2E state.[40]

The assumption that $r = -\sqrt{2}q$ can also be justified for CaO: Cu^{2+}. For strong linear JT coupling and arbitrary warping, r and q are related by the expression[41]

$$r = -q(1 - 3\epsilon)\sqrt{2} , \tag{28}$$

where the parameter ϵ is a function of the ratio of warping to linear JT coupling. Values of ϵ for various ratios of warping to linear JT coupling have been calculated by Williams *et al.*[41] For no warping, $\epsilon \simeq 0.1$, so that $r \simeq -q$. As the ratio of warping increases, ϵ decreases rapidly so that for large warping $r = -\sqrt{2}q$. In the case of CaO: Cu^{2+}, appreciable warping is observed since only one side of the spectrum is affected by random strain coupling to an excited singlet. Thus $r = -\sqrt{2}q$ is a good assumption for CaO: Cu^{2+}. On the other hand, the warping terms for MgO: Cu^{2+} may be weak as evidenced by the possible coupling of both excited singlets to the ground state. For MgO: Cu^{2+}, the relation $r = -q$ may then be more accurate. However, we have found that it is not possible to assume the relation $r = -q$ and describe the MgO: Cu^{2+} spectrum by including random strain coupling to only the A_2 singlet.

The equations from crystal-field theory for the hyperfine interaction which correspond to Eqs. (26)–(27) are as follows[39]:

$$A_1 = -2\mu_B\langle r^{-3}\rangle(\mu/I)(\kappa + 4\lambda/\Delta) , \tag{29}$$

$$A_2 = -2\mu_B\langle r^{-3}\rangle(\mu/I)[\tfrac{1}{7}(4 + 34\lambda/\Delta)] , \tag{30}$$

where $\langle r^{-3}\rangle$ is the mean inverse cube of the $3d^9$ configuration radius, μ is the Cu nuclear magnetic moment, and κ is the Fermi contact parameter. If the measured values of A_1 and qA_2 are substituted into Eqs. (29) and (30) along with the λ/Δ value calculated from g_1, then $\kappa \simeq 0.002$ for CaO: Cu^{2+}. The κ value for MgO: Cu^{2+} is not considered significant since the MgO: Cu^{2+} hyperfine structure could not be explained in detail.

In Table III values of $\bar{\delta}$ and 3Γ are listed that have been determined for Cu^{2+} and Ag^{2+} in the hosts CaO and MgO. The most striking feature of this compilation is that the tunneling splitting is approximately the same for CaO: Cu^{2+}, CaO: Ag^{2+}, and MgO: Ag^{2+}. This similarity in the 3Γ values implies either that the absolute value of both the linear and the warping JT coupling terms is the same in these materials or that the differences which occur in the linear and warping terms between these materials compensate for each other in such a fashion that 3Γ is unchanged. The difference in the ordering of the vibronic singlets that is observed for CaO: Cu^{2+} indicates that the sign of the warping parameter[1] β for CaO: Cu^{2+} is opposite to that for CaO: Ag^{2+} and MgO: Ag^{2+}. This change in the sign of β for CaO: Cu^{2+} coupled with the smaller absolute value of β expected in MgO: Cu^{2+} (as compared with the other materials) indicates that compensating changes in the linear and warping JT terms may be occurring between these materials.

Approximate equality of the respective JT terms in these materials would imply (via the arguments in the Appendix of Ham's review article[1]) that the strain coupling coefficients in these materials have a known proportionate relationship. This in turn would imply that the major differences in the EPR spectra of these materials (other than those due to the differing symmetry properties of the lowest singlet) are due to differing values of average random strain at the impurity site. This possibility could be tested by EPR measurements of uniaxial-stress effects. Raman-scattering experiments on MgO: Cu^{2+}, MgO: Ag^{2+}, and CaO: Ag^{2+} similar to those made by Guha and Chase on CaO: Cu^{2+} would also be extremely helpful in distinguishing the differing roles of the JT coupling terms and random strain in these materials.

TABLE III. Values of average random strain splitting and tunneling splitting determined for d^9 configuration ions in CaO and MgO.

System	Lowest singlet	3Γ (cm^{-1})	$\bar{\delta}$ (cm^{-1})	$\bar{\delta}/3\Gamma$	Ref.
CaO: Cu^{2+}	A_1	≈ 3	2.7	0.67	a
CaO: Cu^{2+}	...	4	...	...	b
CaO: Ag^{2+}	A_2	3.9	4.7	1.2	c, d
MgO: Cu^{2+}	A_2	...	...	0.12[e]	a
MgO: Ag^{2+}	A_2	4.8	0.62	0.13	c

[a]This work.
[b]Reference 38.
[c]Reference 15.
[d]Reference 17.
[e]Note qualification on this measurement as made in text.

V. SUMMARY

The theory of Ham[1] and Chase[14] describing the transition from dynamic to static JT effects in the low-temperature EPR spectra of ^2E orbital states has been entirely successful in explaining the $CaO:Cu^{2+}$ X-band EPR spectrum. Not only has the theory accurately predicted the $(1\bar{1}0)$ and (100) plane angular variations for $CaO:Cu^{2+}$, it has also explained in detail the complicated, asymmetric line shapes observed in the $CaO:Cu^{2+}$ EPR spectrum with $\vec{H} \| \langle 111 \rangle$. The close agreement between theory and experiment for $CaO:Cu^{2+}$ in conjunction with the similar successes obtained in interpreting the $CaO:Ag^{2+}$ and $MgO:Ag^{2+}$ EPR spectra[15,17] provides a convincing validation of the theory. The incomplete explanation of the $MgO:Cu^{2+}$ EPR spectrum does not necessarily represent an inadequacy of the theory but is likely only a reflection of the complexity which results when more than one excited vibronic state is admixed by random strain.

ACKNOWLEDGMENTS

The authors are indebted to Frank S. Ham for his comments and suggestions. Additionally they are grateful to Lloyd L. Chase and S. Guha for communicating their results to them prior to publication. The able technical assistance of E. G. Clardy was also invaluable.

*P.O. Box 6144.
†Operated by Union Carbide Corp. for the USAEC.

[1]For a recent review see F. S. Ham, in *Electron Paramagnetic Resonance*, edited by S. Geschwind (Plenum, New York, 1972).
[2]R. H. Borcherts, H. Kanzaki, and H. Abe, Phys. Rev. B 2, 23 (1970).
[3]G. Kuwabara, J. Phys. Soc. Jap. 31, 1074 (1971).
[4]W. Hayes and J. Wilkins, Proc. R. Soc. Lond. A 281, 340 (1964).
[5]W. Low and J. T. Suss, Phys. Lett. 7, 310 (1963).
[6]J. R. O'Conner and J. H. Chen, Appl. Phys. Lett. 5, 100 (1964).
[7]W. Hayes and J. W. Twidell, Proc. Phys. Soc. Lond. 82, 330 (1963).
[8]F. S. Ham, Phys. Rev. 166, 307 (1968).
[9]J. R. Herrington, T. L. Estle, L. A. Boatner, and B. Dischler, Phys. Rev. Lett. 24, 984 (1970).
[10]U. T. Höchli, Phys. Rev. 162, 262 (1967); see also U. T. Höchli, and T. L. Estle, Phys. Rev. Lett. 18, 128 (1967).
[11]J. R. Herrington, L. A. Boatner, T. J. Aton, and T. L. Estle, Phys. Rev. B 10, 833 (1974).
[12]J. R. Herrington, T. L. Estle, and L. A. Boatner, Phys. Rev. B 7, 3003 (1973).
[13]J. R. Herrington, T. L. Estle, and L. A. Boatner, Phys. Rev. B 3, 2933 (1971).
[14]L. L. Chase, Phys. Rev. B 2, 2308 (1970); L. L. Chase, Phys. Rev. Lett. 23, 275 (1969).
[15]L. A. Boatner, R. W. Reynolds, M. M. Abraham, and Y. Chen, Phys. Rev. Lett. 31, 7 (1973).
[16]L. A. Boatner, R. W. Reynolds, M. M. Abraham, and Y. Chen, Bull. Am. Phys. Soc. 18, 448 (1973).
[17]R. W. Reynolds, L. A. Boatner, M. M. Abraham, and Y. Chen, Bull. Am. Phys. Soc. 19, 326 (1974).
[18]R. W. Reynolds, L. A. Boatner, M. M. Abraham, and Y. Chen, Bull. Am. Phys. Soc. 18, 448 (1973).
[19]J. H. Van Vleck, Phys. Rev. 52, 246 (1937); J. Chem. Phys. 7, 61 (1939); 7, 72 (1939).
[20]A. D. Liehr and C. J. Ballhausen, Ann. Phys. (N.Y.) 3, 304 (1958).
[21]U. Öpik and M. H. L. Pryce, Proc. R. Soc. Lond. A 238, 425 (1957).
[22]I. B. Bersuker, Zh. Eksp. Teor. Fiz. 43, 1315 (1962) [Sov. Phys.-JETP 16, 933 (1963)].
[23]I. B. Bersuker and B. G. Vekhter, Fiz. Tverd. Tela 5, 2432 (1963) [English Translation: Soviet Phys.-Solid State 5, 1772 (1964)].
[24]M. C. M. O'Brien, Proc. R. Soc. Lond. A 281, 323 (1964).
[25]F. S. Ham, Phys. Rev. 138, A 1727 (1965).
[26]W. Moffitt and A. D. Liehr, Phys. Rev. 106, 1195 (1957); W. Moffitt and W. Thorson, *ibid.* 108, 1251 (1957).
[27]H. C. Longuet-Higgins, U. Opik, M. H. L. Pryce, and R. A. Sack, Proc. R. Soc. Lond. A 244, 1 (1958).
[28]J. R. Herrington, T. L. Estle, and L. A. Boatner, Phys. Rev. B 5, 2500 (1972).
[29]W. Low and J. T. Suss, Solid State Commun. 2, 1 (1964); R. W. Reynolds, L. A. Boatner, Y. Chen, and M. M. Abraham, J. Chem. Phys. 60, 1593 (1974).
[30]L. A. Boatner and R. W. Reynolds, Bull. Am. Phys. Soc. 19, 326 (1974).
[31]J. W. Orton, P. Auzins, J. H. E. Griffiths, and J. E. Wertz, Proc. Phys. Soc. Lond. 78, 554 (1961).
[32]R. E. Coffman, J. Chem. Phys. 48, 609 (1968).
[33]R. E. Coffman, D. L. Lyle, and D. R. Mattison, J. Phys. Chem. 72, 1392 (1968).
[34]R. Englman, Phys. Lett. 31, 473 (1970).
[35]K. Žďánský, Phys. Rev. 177, 490 (1969).
[36]U. Höchli, K. A. Müller and P. Wysling, Phys. Lett. 15, 5 (1965).
[37]M. M. Abraham, C. T. Butler, and Y. Chen, J. Chem. Phys. 55, 3752 (1971).
[38]S. Guha and L. L. Chase, Phys. Rev. Lett. 32, 869 (1974).
[39]A. Abragam and M. H. L. Pryce, Proc. R. Soc. Lond. A 63, 135 (1951).
[40]B. Halperin and R. Englman, Phys. Rev. B 9, 2264 (1974).
[41]F. I. B. Williams, D. C. Krupka, and D. P. Breen, Phys. Rev. 179, 255 (1969).